(A New Proposal to Jefferson Lab PAC27)
Neutron Tagged bound proton structure to probe the Origin of the EMC Effect

G.D. Cates, D. Day, N. Liyanage (Spokesperson and contact person),
R. Lindgren, V. Nelyubin, B. Norum, O. Rondon, K. SLifer, A. Tobias, K. Wang,
S. Tajima, B. Craver, R. Chang
University of Virginia, Charlottesville, VA 22904

J.P. Chen, P. Degtiarenko, E. Chudakov, J. Gomez, O. Hansen, D. Higinbotham, B. Reitz,
B. Wojtsekhowski (Spokesperson)
Jefferson Lab, Newport News, VA 23606

J. R. Arrington, K. Hafidi, R. J. Holt, D. H. Potterveld, P. E. Reimer,
E. C. Schulte, X. Zheng.
Argonne National Laboratory, Argonne, IL 60439

W. Berttozi, O. Gayou, S. Gilad,A.J. Puckett,Y. Qiang, X. Zhan
Massachusetts Institute of Technology, Cambridge, MA 02139

B. Sawatzky
Temple University, Philadelphia, PA 19122

J.R.M. Annand
University of Glasgow, Glasgow G128QQ, Scotland, UK

R. Gilman, X. Jiang, E. Kuchina, R. Ransome,
Rutgers University, Piscataway, NJ 08855

H. Gao, D. Dutta, K. Kramer, X. Qian, W. Chen
Duke University, Durham, NC 27708

D. T. Averett
College of William and Mary, Williamsburg, VA 23185

K. Wijesooriya
Virginia Commonwealth University, Richmond, VA 23284

A Hall A Collaboration Proposal

December 6, 2004

Abstract

Deep inelastic scattering of high energy electrons off a proton bound in a deuteron in coincidence with a slow backward going neutron will be investigated in Hall A using the large acceptance BigBite spectrometer. We will study the variation of the ratio of the bound proton cross section to the free proton cross section over a grid of the scaling variable x and the recoil neutron momentum up to $x \approx 0.6$ in the deep inelastic scattering region. This is a novel and a sensitive way to study the EMC effect that has been advocated by the theory community for many years. This experiment will provide crucial evidence needed to distinguish between possible mechanisms responsible for the EMC effect.

1 Introduction

It has been more than two decades since the discovery of the EMC effect. However, its origin still remains a mystery. There are many theoretical models that attempt to explain the EMC effect. They range from models that explain the EMC effect entirely in terms of hadronic degrees of freedom of the nuclear force to those that attribute the effect to the deformation of the nucleonic wave function. Since the publication of the EMC data in 1983 [1], there have been many precision inclusive measurements of the EMC effect on various nuclear targets over a large range of x and Q^2 [2, 3, 4, 5]. This large collection of data has revealed several important facts about the EMC effect:

- the x dependent shape of the EMC effect is roughly independent of the target atomic mass number, A,
- the increase in the EMC effect at a given x with increasing A can be described well as a function of A or as a linear function of nuclear density,
- the EMC effect does not depend on Q^2.

For a review of the published EMC effect data and theoretical models, see [6]. Hall C Experiment E03-013 [7] is currently collecting inclusive data for a precision measurement of the EMC effect on ^3He and ^4He.

The models based on very different physics ideas can more or less fit the x and the A dependence of the EMC effect. Therefore is has not been possible to distinguish between the models to identify a possible cause of the EMC effect. What has been missing in the available data-sets is a measurement of the variation of the effect as the binding of the nucleon increases and it becomes more and more off-shell. In the case of the deuteron, the recoil momentum of the spectator nucleon is a measure of the nuclear binding strength. A comparison of several available EMC effect models by Melnitchouk, Sargsian and Strikman [8] has indicated that the models based on different physics ideas make vastly different predictions for the EMC effect as a function of the nuclear binding strength (or the recoil momentum of the spectator in case of the deuteron). Therefore, a precision measurement of the EMC effect for the bound proton in a deuteron as a function of the recoil neutron momentum can be used to distinguish between different classes of models. This may help us understand the origins of the EMC effect.

At Jefferson Lab Hall A we can measure the ratio of the cross section for a bound proton in a deuteron to that of a free proton as a function of the recoil neutron momentum at different values of x, up to $x \approx 0.6$, in the DIS region ($1 < Q^2 < 5$ $(\mathrm{GeV}/c)^2$ and $W^2 > 4$ GeV^2). The accessible range of the recoil neutron momentum would be from as low as 50 to 60 MeV/c, where the proton is expected to be barely bound, to about 400 MeV/c, where the proton is significantly off-shell. We will select extreme backward kinematics and a low transverse momentum for the recoil neutron detection. The neutron is in spectator kinematics in this case. Furthermore, Final State Interaction (FSI) effects have been predicted to be minimal for these kinematics [8]. Since it is the point-to-point variation of the EMC effect for the

bound proton that is interesting, we will form the ratio of the bound proton cross-section at different values of x to the bound proton cross-section measured at $x = 0.2$, where the EMC effect is minimal. Forming this cross section ratio would divide out experimental systematics such as the neutron detection efficiency as well as theoretical uncertainties such as the dependence on the deuteron wave function. In this proposal we will demonstrate that we can measure the relevant cross section ratio with high accuracy over a fine grid of x and the recoil neutron momentum.

Jefferson Lab Hall B experiment E-94-102 [9] recently measured the cross section for the bound neutron in the deuteron by tagging the proton over the recoil momentum range of 250 MeV/c to 400 MeV/c. However in this case there is no free neutron cross section to compare the bound cross section to and hence one has to rely on models to estimate the degree of the EMC effect as a function of the recoil momentum. In contrast, in the proposed experiment the ratio of the bound cross section to the free cross section allows us to estimate the level of the EMC effect in a model independent way. Furthermore in the proposed experiment we will detect the spectator neutrons down to a recoil momentum of 50 to 60 MeV/c, which corresponds to barely 1-2 MeV in kinetic energy. This would allow us to study the evolution of the EMC effect from a barely bound to a strongly bound proton.

While it is vitally important to understand the origin of the EMC effect in its own right, it is also important for the extraction of the neutron structure functions from nuclear targets. An unambiguous measurement of the F_2^n/F_2^p ratio is of fundamental importance, as has been pointed out at Jefferson Lab many times over the last few years. It is the EMC effect in the deuteron that prevents an unambiguous extraction of F_2^n at large values of x [10]. The Hall B BoNuS experiment [12] plans to measure the proton tagged F_2^n at low recoil momenta ($P > 70$ MeV/c) to minimize nuclear effects. While the nuclear effects are expected to be generally small in the momentum range of the BoNuS experiment ($P \approx 100$ MeV/c), different models of the EMC effect predict different levels of effect, ranging from less than 1% to about 3-4% level for $x \approx 0.6$. Once again, since there is no free nucleon measurement to compare to, one has to rely on theoretical models to correct for this effect. On the other hand, using the proposed experiment we can accurately measure the level of the EMC effect for the proton over the recoil momentum range of the BoNuS experiment, and then one can use these data to constrain the models to perform more effective corrections to the F_2^n data. The influence of the EMC effect on the F_2^n results has been shown to increase rapidly with increasing x. Since measuring the F_2^n/F_2^p ratio as $x \to 1$ is one of the major experimental initiatives for the CEBAF 12 GeV upgrade, understanding the evolution of the EMC effect as a function of the spectator momentum would be of great importance to the 12 GeV program.

2 The Formalism

2.1 Inclusive Deep Inelastic Scattering

The inclusive cross section in the DIS region can be written in terms of the structure functions F_1 and F_2 as

$$\frac{\mathrm{d}^2\sigma}{\mathrm{d}\Omega \mathrm{d}E'} = \left(\frac{\mathrm{d}\sigma}{\mathrm{d}\Omega}\right)_{Mott}\left[\frac{1}{\nu}F_2(x,Q^2) + \frac{2}{M}F_1(x,Q^2)\tan^2\frac{\theta}{2}\right] , \tag{1}$$

where θ is the scattering angle of the electron in the laboratory frame. The four momentum transfer squared, $Q^2 = -q^2$, is given by

$$Q^2 = 4EE'\sin^2\frac{\theta}{2} , \tag{2}$$

scaling variable x,

$$x = \frac{Q^2}{2p\cdot q} , \tag{3}$$

(p is the initial four momentum of the struck nucleon) and the Mott cross section,

$$\left(\frac{\mathrm{d}\sigma}{\mathrm{d}\Omega}\right)_{Mott} = \frac{\alpha^2\cos^2\frac{\theta}{2}}{4E^2\sin^4\frac{\theta}{2}} = \frac{\alpha^2\cos^2\frac{\theta}{2}}{Q^4}\frac{E'}{E} \tag{4}$$

where α is the fine structure constant. $F_1(x,Q^2)$ and $F_2(x,Q^2)$ are related to each other through R, the ratio between longitudinal and transverse virtual photon cross sections,

$$F_1(x,Q^2) = \frac{F_2(x,Q^2)(1+\gamma^2)}{2x\Big(1+R(x,Q^2)\Big)} \tag{5}$$

where $\gamma^2 = (2Mx)^2/Q^2$.

Thus in the case of inclusive scattering off a free proton, the structure function $F_2(x,Q^2)$ can be extracted from the cross section:

$$F_2^{free}(x,Q^2) = \left[\frac{d^2\sigma/d\Omega dE'}{(d\sigma/d\Omega)_{Mott}}\right]\left[\frac{\nu\epsilon(1+R(x,Q^2))}{1+\epsilon R(x,Q^2)}\right] \tag{6}$$

2.2 Spectator tagging measurement

A convenient choice of independent variables for a spectator tagging measurement includes Q^2 and x, as well as the transverse momentum p_t^{sp} and the light cone momentum fraction α^{sp} of the spectator nucleon.

$$\alpha^{sp} = \frac{E^{sp} - p_z^{sp}}{M}$$

where p_z^{sp} is the spectator momentum along the q vector. The detection of the recoil nucleon in extreme backward angles such that $p_t \approx 0$ ensures that FSI effects

are minimal and the recoil nucleon was in spectator kinematics. For this kinematic arrangement $\alpha^{sp} \geq 1$.

When the struck nucleon is initially at rest $p \cdot q = M\nu$ (where ν is the energy transfer in the lab frame) and x is given by

$$x = \frac{Q^2}{2p \cdot q} = \frac{Q^2}{2M\nu} = x_{Bj} \ , \tag{7}$$

and $W^2 = (q+p)^2$, the total hadronic mass squared, is given by

$$W^2 = M^2 - Q^2 + 2p \cdot q = M^2 - Q^2 + 2M\nu \ , \tag{8}$$

However, when the electron scatters off a bound nucleon moving with a momentum $\vec{p}$, where $\vec{p} = -\vec{p}^{sp}$ in the spectator picture, x and W^2 are different from x and W^2 calculated in equations 7 and 8 assuming a nucleon stationary in the lab frame. Thus in this proposal we use the notation

$$x' = \frac{Q^2}{2p \cdot q} \ , \tag{9}$$

and

$$W'^2 = M^2 - Q^2 + 2p \cdot q \ , \tag{10}$$

and explicitly calculate x' and W'^2 for each α^{sp} bin using the spectator picture: $\vec{p} = -\vec{p}^{sp}$. Note that in the limit $q/\nu \to 1$, x' is related to x_{Bj} by

$$x' \approx \frac{x}{2 - \alpha^{sp}} \ . \tag{11}$$

In the nuclear impulse approximation, where incoherent inelastic scattering takes place from individual nucleons in the nucleus, the semi-inclusive cross section for the reaction D$(e,e'$N$)$X can be written as a product of the deuteron spectral function $S(\alpha^{sp}, p_t)$ and the effective structure function $F_{2,p}^{eff}$ [31, 8]

$$\frac{d\sigma^{eD \to enX}}{dx dW^2 d(\log \alpha^{sp}) d^2p_t} \approx \frac{2\alpha_{em}^2}{Q^4}(1-y) S(\alpha^{sp}, p_t) F_{2,p}^{eff} \left(\frac{x}{2 - \alpha^{sp}}, p_t, Q^2 \right) \tag{12}$$

From equations 6 and 12 we see that one can access the ratio $F_{2,p}^{eff}/F_{2,p}^{free}$ through,

$$\frac{F_{2,p}^{eff}}{F_{2,p}^{free}} \propto \frac{\sigma(D(e,e',N)X)_{x',\alpha^{sp},p_t,Q^2)}}{\sigma(p(e,e')X)_{(x',Q^2)}}. \tag{13}$$

However there are practical difficulties in accessing $F_{2,p}^{eff}$ from a D$(e,e'$n$)$X absolute cross section measurement. The uncertainties in spectator neutron detection efficiency and solid angle will dominate the uncertainty of this cross section measurement. Even if such an absolute semi-inclusive cross section were measured, the uncertainty in the deuteron spectral function would dominate the uncertainly in extracted $F_{2,p}^{eff}$, especially at high recoil momenta.

However, we can take advantage of the fact that these uncertainties are only dependent on the spectator neutron momentum; they are not correlated with x or Q^2 for the electron scattering off the proton. Thus, all these uncertainties can be divided out by forming the ratio between D$(e,e'$n$)$X cross section at a given x' and D$(e,e'$n$)$X cross section at $x' = 0.2$, where the observed EMC effect in inclusive scattering is small

$$\begin{aligned} G(\alpha^{sp}, p_t, x'_1, x'_2, Q^2) &\equiv \frac{d\sigma(x_1, \alpha^{sp}, p_t, Q^2)}{dx dW^2 d(\log \alpha^{sp}) d^2\mathbf{p}_t} \Big/ \frac{d\sigma(x_2, \alpha^{sp}, p_t, Q^2)}{dx dW^2 d(\log \alpha^{sp}) d^2\mathbf{p}_t} \\ &= \frac{F_{2,p}^{eff}(x'_1, p_t, Q^2)}{F_{2,p}^{eff}(x'_2, p_t, Q^2)}. \end{aligned} \tag{14}$$

where $x'_2 = 0.2$.

Furthermore, the FSI effects on the spectator are expected to be independent of x [32, 8]. Thus, the above ratio will divide out FSI providing a much cleaner way to access information on $F_{2,p}^{eff}$ than through an absolute cross section measurement.

In [8] Melnitchouk *et al.* compared the predictions from three different classes of EMC effects models for the ratios $F_{2,p}^{eff}/F_{2,p}^{free}$ and $G(\alpha^{sp}, p_t, x_1, x_2, Q^2)$ as a function of α^{sp}. The models they considered were:

- **Binding Models**: There are many theoretical models [23, 35, 36, 37, 38, 39, 40, 41, 42] that try to explain the main features of the EMC effect in terms of conventional nuclear degrees of freedom, nucleons and pions, responsible for the binding in nuclei. In many of these models the structure functions of the bound nucleon only plays a minor role.

- **Color Screening Model of Suppression of Point-Like Configurations (PLC) in Bound Nucleons** The increase in the EMC effect with x may indicate that the high momentum components of the quark distribution in the nucleon might play an important role in the EMC effect. For these high momentum configurations the three quarks are likely to be close together. In the Color Screening Model of Frankfurt and Strikman [23, 31] they assume that for large x the dominant contribution to $F_{2,N}(x, Q^2)$ is given by the Point-Like Configurations (PLC) of partons which weakly interact with the other nucleons. They argue that the suppression of this component in a bound nucleon is the main source of the EMC effect.

- **Rescaling model, QCD Radiation - Quark Delocalization**: Some authors have argued[46, 48, 49, 50] that due to the quark delocalization (or enlargement -swelling- of the confinement radius) of a bound nucleon, it radiates gluons more efficiently than a free nucleon. In this model the strength is shifted in x due to this extra gluon radiation when the electron scatters off a bound nucleon.

Figures 1 and 2 show the comparison between these predictions at $x = 0.6$. As figure 2 indicates, a measurement of $G(\alpha^{sp}, p_t, x_1, x_2, Q^2)$ vs. α^{sp} will clearly distinguish between models of the EMC effect.

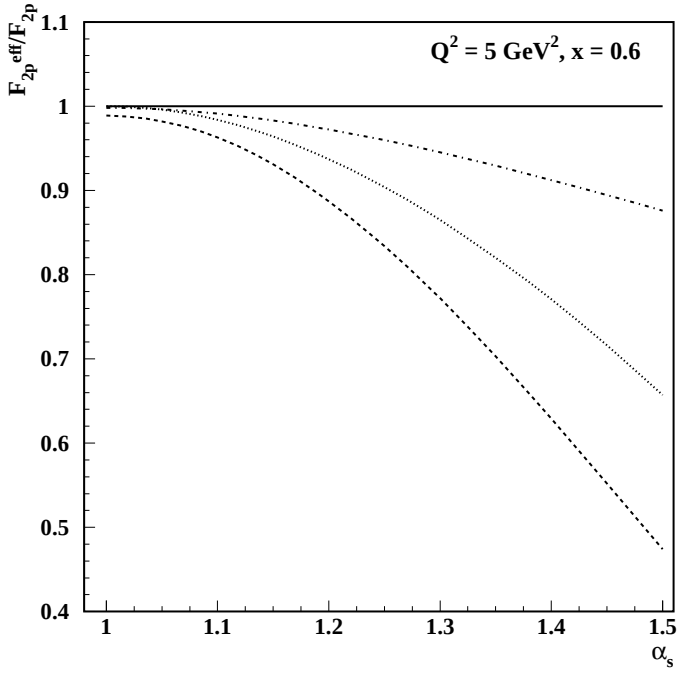

Figure 1: The α^{sp} dependence of $F_{2,p}^{eff}/F_{2,p}^{free}$ ratio at $x = 0.6$ from [8]. The dashed line is the PLC suppression model, dotted is the rescaling model and dot-dashed the Binding model.

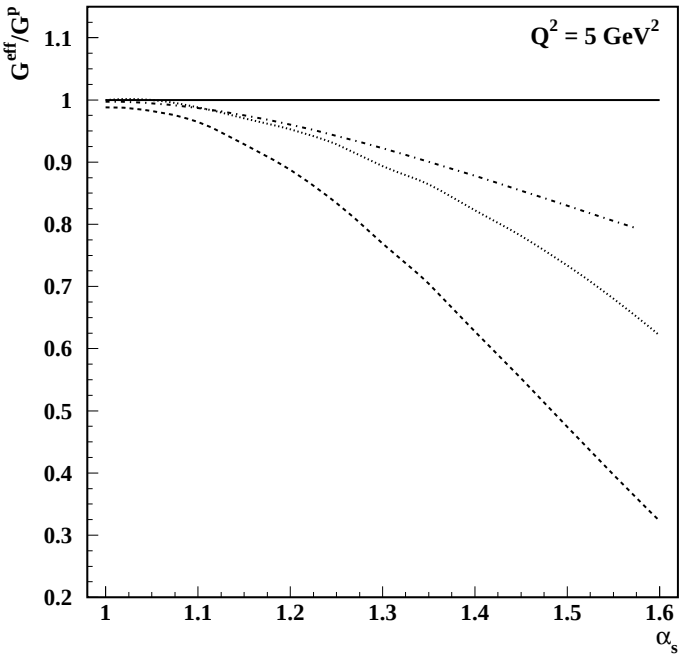

Figure 2: The α^{sp} dependence of $G(\alpha^{sp}, p_t, x_1, x_2, Q^2)$ with $x_1 = x/(2-\alpha^{sp}) = 0.6$ and $x_2 = x/(2-\alpha^{sp}) = 0.2$, for $p_t = 0$. $G^{eff}(\alpha^{sp}, p_t, x_1, x_2, Q^2)$ is normalized to $G^p(\alpha^{sp}, p_t, x_1, x_2, Q^2)$ calculated with the free nucleon structure function. The dashed line is the PLC suppression model, dotted is the rescaling model and dot-dashed the Binding model.

3 The Experiment

We are proposing to measure a semi-inclusive $D(e,e'n)X$ cross section ratio over a grid of x' and α^{sp} to access the structure function ratio $G(\alpha^{sp}, p_t, x'_1, x'_2, Q^2)$ defined in equation 14. Each of the two semi-inclusive $D(e,e'n)X$ cross sections going into the ratio will be normalized to inclusive $D(e,e')$ cross sections as outlined below.

- We will use inclusive $D(e,e')$ data we gather simultaneously with $D(e,e'n)X$ coincidence data to normalize the $D(e,e'n)X$ cross section.
- The $D(e,e'n)X$ and $D(e,e')$ raw yields will be divided into E', θ and ϕ bins over the BigBite acceptance using identical cuts. Then the $D(e,e'n)X$ yield will be divided by the $D(e,e')$ yield bin by bin. This division will remove all normalization uncertainties on the electron detection side such as the luminosity, BigBite acceptance and efficiency. The world cross section data for $D(e,e')$ evaluated at each E', θ and ϕ bin normalizes the the $D(e,e'n)X$ cross section for that bin.
- The normalized $D(e,e'n)X$ yield will then be divided into x' and α^{sp} bins. At each α^{sp} bin, the normalized yield from different bins in x' will be divided by the normalized yield from the $x' = 0.2$ bin. This normalization will divide out the deuteron spectral function, neutron detection efficiency and neutron detector solid angle at each α^{sp} bin. Thus this final ratio of $D(e,e'n)X$ yields will be equal to the cross section ratio

$$G = \frac{\sigma(D(e,e'n)X)_{(x'_1,\alpha^{sp},p_t,Q^2_1)}}{\sigma(D(e,e'n)X)_{(x'_2=0.2,\alpha^{sp},p_t,Q^2_2)}} \tag{15}$$

  within a systematic uncertainty only limited by the inclusive $D(e,e')$ structure function world data. In the kinematic region of the proposed experiment, these structure functions are known approximately to 1% level [57].

In the next few sections we address the remaining important issues related to the spectator nucleon approach:

3.1 Final State Interaction and p_t dependence issues

In the extreme backward neutron kinematics we are proposing for this experiment the FSI - the re-scattering of the spectator neutron by the remnants of the struck proton - have been shown to be suppressed [29, 30, 32]. An estimate made by Melnitchouk *et al* for extreme backward kinematics indicates that for small p_t ($p_t \approx 0.1$ GeV) and $\alpha^{sp} < 1.5$, the FSI contribution to $D(e,e'n)X$ is less than 5%. A recent analysis of of the effects of FSI on the spectator nucleon has confirmed that these effects are practically independent of x' and Q^2 [32]. Therefore any FSI effects remaining in the kinematics of our experiments will be divided out when we form the ratio G

The proposed neutron detection system for this experiment covering the backward hemisphere is optimized to detect neutrons with low p_t. Furthermore, we have used

a kinematic cut at $p_t < 0.2$ GeV in our rate estimates and will use a similar cut in the data analysis to remove high p_t neutrons. For low α^{sp} bins we will further bin the data in several p_t bins to study the p_t dependence. If there is larger than expected dependence on p_t, this study will allow us to use more restrictive cuts to limit the data to even smaller values of p_t and to interpolate the measured values to $p_t = 0$.

3.2 Neutron creation due to target fragmentation and the Sullivan process

The fragmentation of low momentum neutrons from the proton debris is strongly suppressed in the extreme backward neutron kinematics [52, 56]. The contamination of spectator neutrons due to target fragmentation is expected to be negligible for the kinematics of the proposed experiment.

Another possible way to get a slow backward going neutron is through the Sullivan process, where the electron scatters off a π^+ in the pion cloud of the proton or off a π^0 in the pion cloud of the neutron. The cross section for this process was measured through leading neutron detection at HERA [58]. The contamination of spectator neutrons due to DIS off a pion in the pion cloud was calculated for the proposed kinematics using the prescription by Melnitchouk and Thomas [11]. This calculation shows that the contamination is less than 2.5% in our kinematics: changing from about 1.5 % at at $x' = 0.2$ to practically zero at $x' = 0.6$.

We will measure the level of contamination due to target fragmentation and the Sullivan process during our experiment by measuring the $H(e, e'n)X$ cross section with the neutron detection system in the identical configuration to the deuterium runs. This will allow us correct these small contaminations with a high accuracy.

The cross section data for the Sullivan process has been incorporated into a *ep* collision Monte-Carlo Simulation program **RAPGAP** [59]. We will use the results from the $H(e, e'n)X$ run to calibrate **RAPGAP** simulation for our kinematics and then will use it to correct the measured $D(e, e'n)X$ cross sections bin by bin.

3.3 Experimental Setup

We will use a beam energy of 6 GeV. A low average beam current of 0.8 μA and a thin - 1 cm long - liquid deuterium target would be used to achieve a luminosity of 5×10^{35} cm^{-2}s^{-1}. The experimental setup is shown in the schematic diagram of figure 3. The scattered electrons will be detected in the BigBite spectrometer at 35°. The backward going recoil neutrons will be detected using a combination of a especially designed low energy neutron detector and the GEN neutron detector [51].

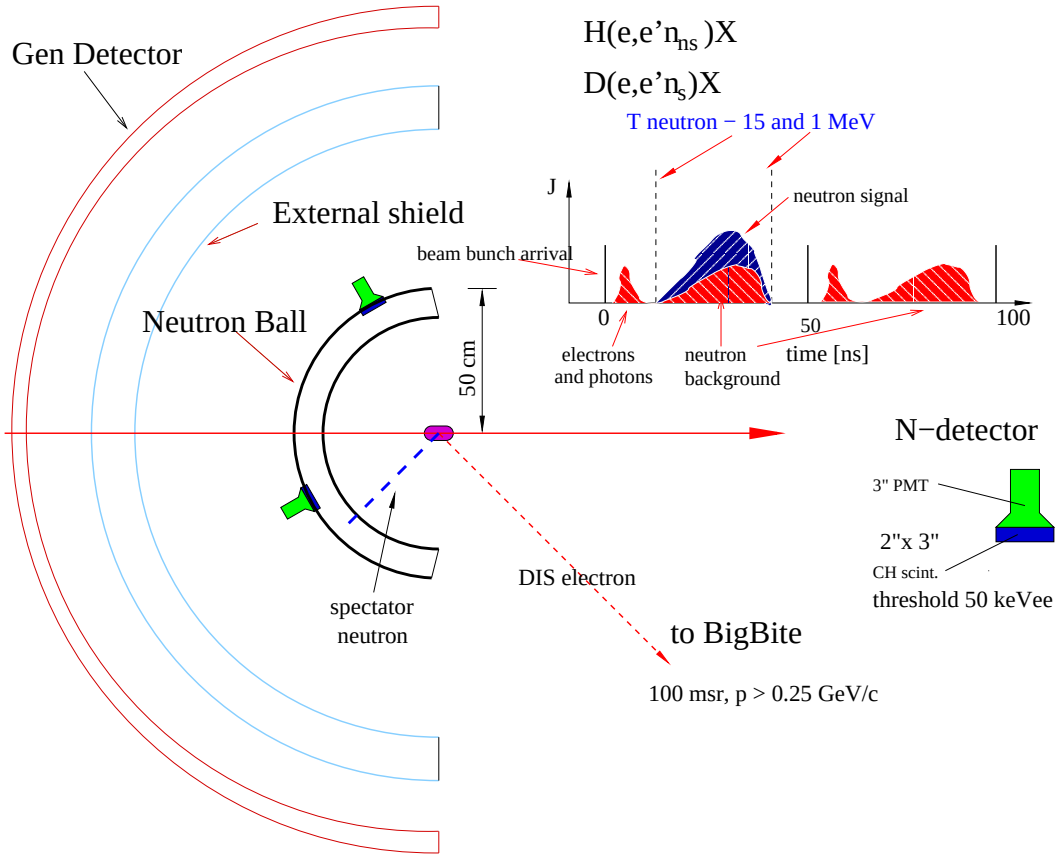

Figure 3: Schematic diagram of the proposed experimental setup

3.4 Liquid deuterium target cell

In principle we can use the standard 4 cm liquid deuterium target cell for this experiment. However the low luminosity required for this experiment combined with a 4 cm target restricts the average beam current to 0.2 μA. A current that may be too low for Hall A beam line equipment to work properly. While we are not sensitive to beam current measurements, we need to keep good control over beam position to keep background down. Furthermore, a shorter target reduces the probability of secondary electrons from creating more background.

We feel that these physics reasons are strong enough to justify the extra effort to design and construct a new 1 cm target cell unit for the Hall A cryo target. We are proposing a 1 cm diameter vertical flow cylindrical cell with 2 μm stainless steel walls. Such cells have been used previously for experiments at MIT-Bates. The cell wall contribution will be at approximately 2% of the signal and will be corrected accurately using data from an empty target run.

3.5 BigBite Spectrometer

The electrons will be detected in the BigBite spectrometer. The large angular and momentum acceptances of BigBite provide a combined gain factor of 30-50 in comparison with the Hall A High Resolution Spectrometers (HRS). This is the first key experimental factor that makes the proposed experiment possible. Large acceptance allows us to use the low luminosity required for very slow neutron detection. Furthermore, due to the wide momentum acceptance of BigBite, all the data will come from a single field setting of the spectrometer. In the proposed momentum range, 0.5 GeV/c to about 2.0 GeV/c, the momentum resolution of the BigBite spectrometer would be between 0.5% and 1.5%. This is sufficient for the proposed measurement which relies on normalization to the free proton.

Due to the relatively low luminosity, the expected rates in the BigBite detectors for this experiment is much lower than the rates for other BigBite experiments.

The only new addition to the BigBite spectrometer required for this experiment is a gas Čerenkov counter. The worst case pion to electron ratio we expect for this experiment is about 10:1. With the combination of a gas Čerenkov counter and the BigBite shower counter, which is already under construction, we plan to achieve a pion rejection ratio of about 1000. This is more than adequate to reject the pions for this experiment.

3.5.1 Shower detector

The shower detector for the BigBite spectrometer is under construction by the GEn collaboration. It consists of the preshower and shower sections made out of lead-glass counters. A total of 250 counters are used in that detector. A pion rejection factor of 30 is expected for this detector with an electron detection efficiency of 98%.

3.5.2 Gas Čerenkov counter

For the high luminosity of $1{\cdot}10^{37}$ cm^{-2}s^{-1} expected in the GEn experiment the BigBite detector package includes three drift chambers. The role of the middle chamber is to ensure multi-track reconstruction at high rates. At the luminosity of the proposed experiment we can remove the middle chamber. The space between the remaining chambers of 60 cm allows insertion of a 50-60 cm gas Čerenkov counter with an expected pion rejection factor of roughly 100. We plan to use a configuration similar to the Hall A HRS gas Čerenkov counters with segmentation into 10 PMTs. The expected cost of this detector is less than \$50k.

3.6 Recoil neutron detection

The second key experimental component of our proposal, which allows us to use sufficiently high luminosity, is a low duty factor regime of the electron beam. The G0 experiment successfully used a beam structure with pulses 32 ns apart. An even

larger time structure of 48 ns[1] will be used in our experiment.

For detection of neutrons with kinetic energies between 1 MeV and 15 MeV ($50 < p^{sp} < 170$ MeV/c), we are proposing to construct a special low energy neutron detector - neutron hemisphere - based on liquid or plastic scintillators. This detector would be placed at 50 cm from the target to cover most of the backward hemisphere. The total solid angle would be approximately 4 sr. A 5 mm thick lead shield will be installed in front of the detector to stop low-energy charged particles, and to suppress very low-energy photon flux.

A Monte-Carlo calculation performed for the proposed neutron detector[54] indicates that with a 50 keVee threshold on neutron detectors we can detect neutrons down to about 1 MeV kinetic energy.

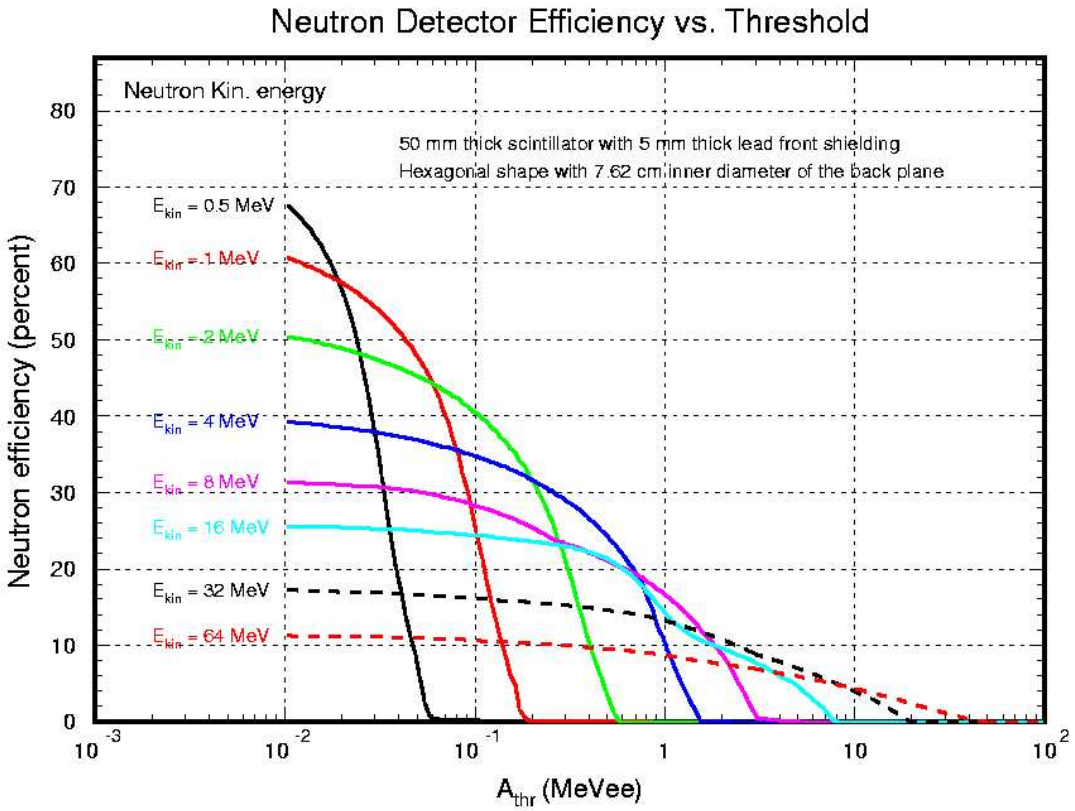

Figure 4: Preliminary MC results for neutron efficiency.

At a luminosity of 5×10^{35} cm^{-2}s^{-1} the amount of background of neutral and charged particles was found from MC simulations preformed by Pavel Degtiarenko [55] (see figures 5- 8). The rates of all other particles at the neutron detector have negligible effects for the proposed experiment and are not shown. A few nanoseconds after the beam bunch passes through the target, the photons and most of the other particles will pass through the neutron detectors. These fast particles can be cleanly

[1] This corresponds to a pulse rate of 20 MHz. If accelerator technical issues force us to use a 16 MHz structure, it will change the projections presented here only by a small amount.

separated from the slow neutrons using time of flight. Thus the only effect these particles have on our experiment is through making the neutron cells they hit go dead for about 30-50 ns after the hit. With a beam pulse frequency of 20 MHz and a segmentation of the neutron detector into 175 counters any particle type with less than 20 MHz background rate at the detectors will have less than 1% contribution towards this deadtime. As the figures 5- 7 show only 1-2 MeV electrons will have any significant contribution. With a flux of these electron of the order 100 MHz, there will be about five hits on the neutron detector per pulse. These will occupy five out of 175 detection cells for 30-50 ns, causing a deadtime of the order 3-5%. This dead time will be accurately measured and corrected.

Neutrons with kinetic energies between 1 MeV and 15 MeV will arrive at the detector between 9 ns and 31 ns after the beam bucket. The soft protons having been stopped by the lead shield, the main background in that time interval will be low energy neutrons.

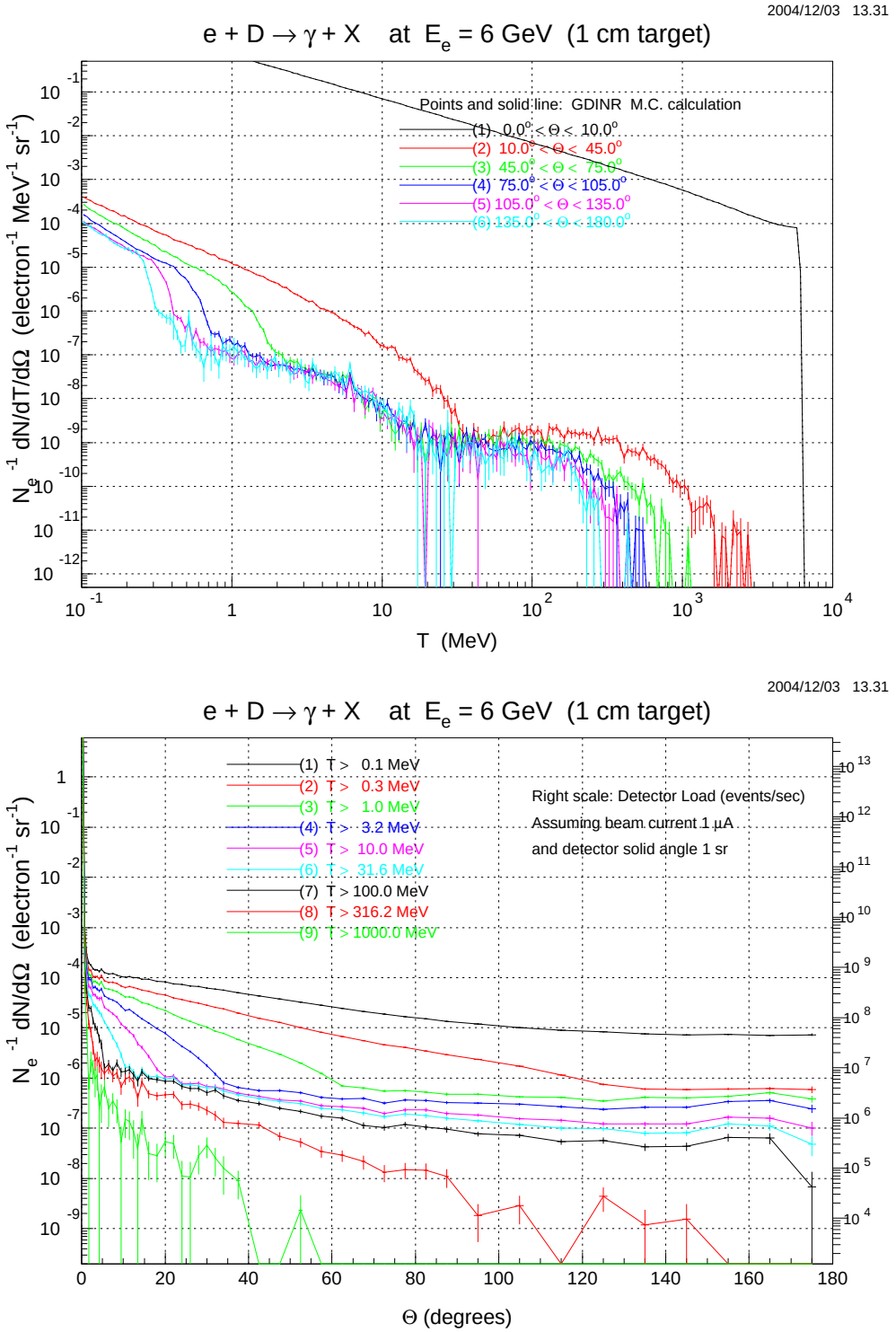

Figure 5: Monte-Carlo results for photon background for the proposed experiment per sr. The 5 mm lead shield will stop all 0.1 MeV photons and will reduce the flux of 0.3 MeV photons by a factor of 300. Thus the effective photon flux at the neutron detector will be below 5 MHz. Note that the luminosity used in these simulations is higher than 5×10^{35} cm^{-2}s^{-1}.

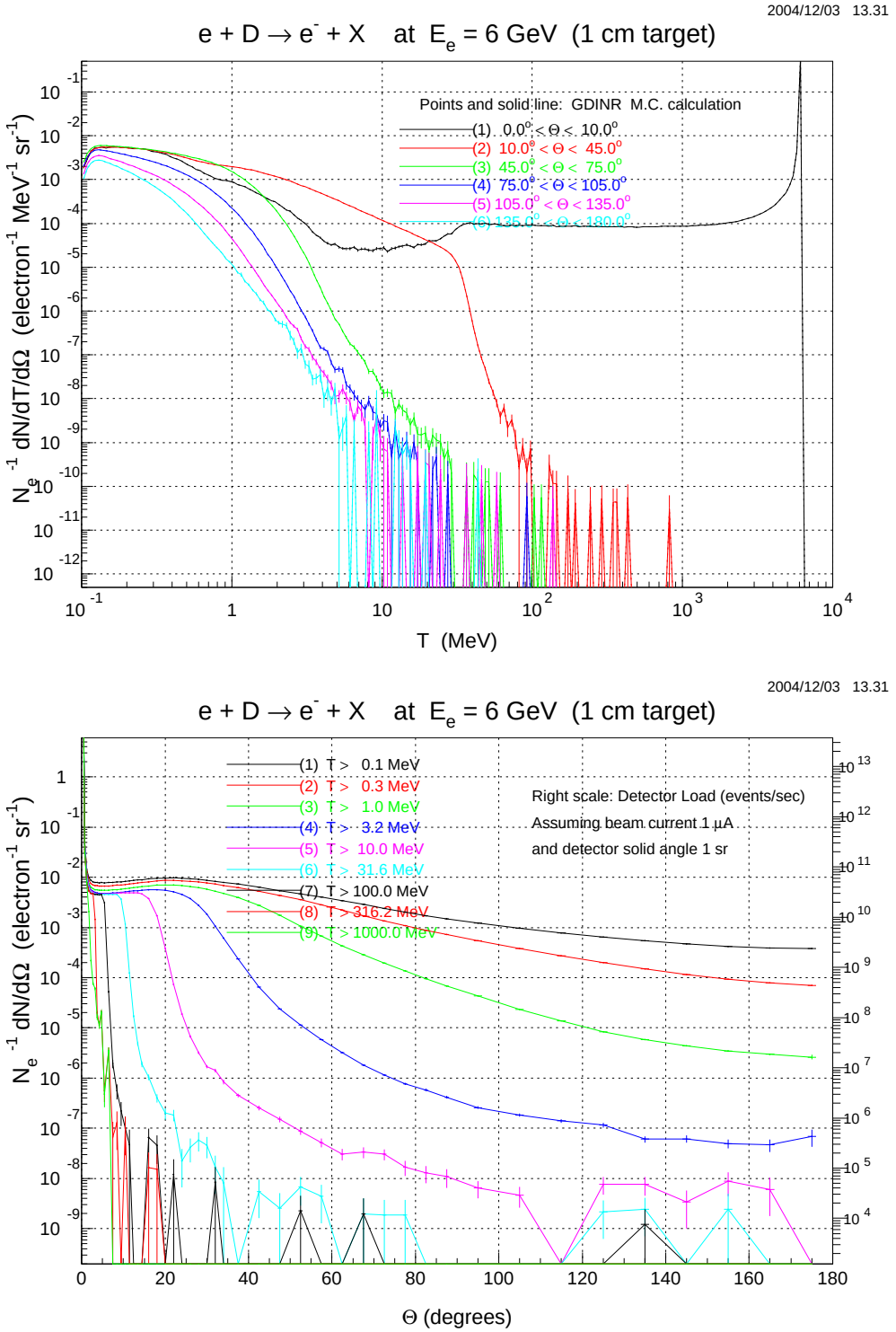

Figure 6: Monte-Carlo results for electron background for the proposed experiment per sr. The 5 mm lead shield will stop electrons with kinetic energies less than $\approx$ 1 MeV. Thus the effective electron flux at the neutron detector will be less than 100 MHz.

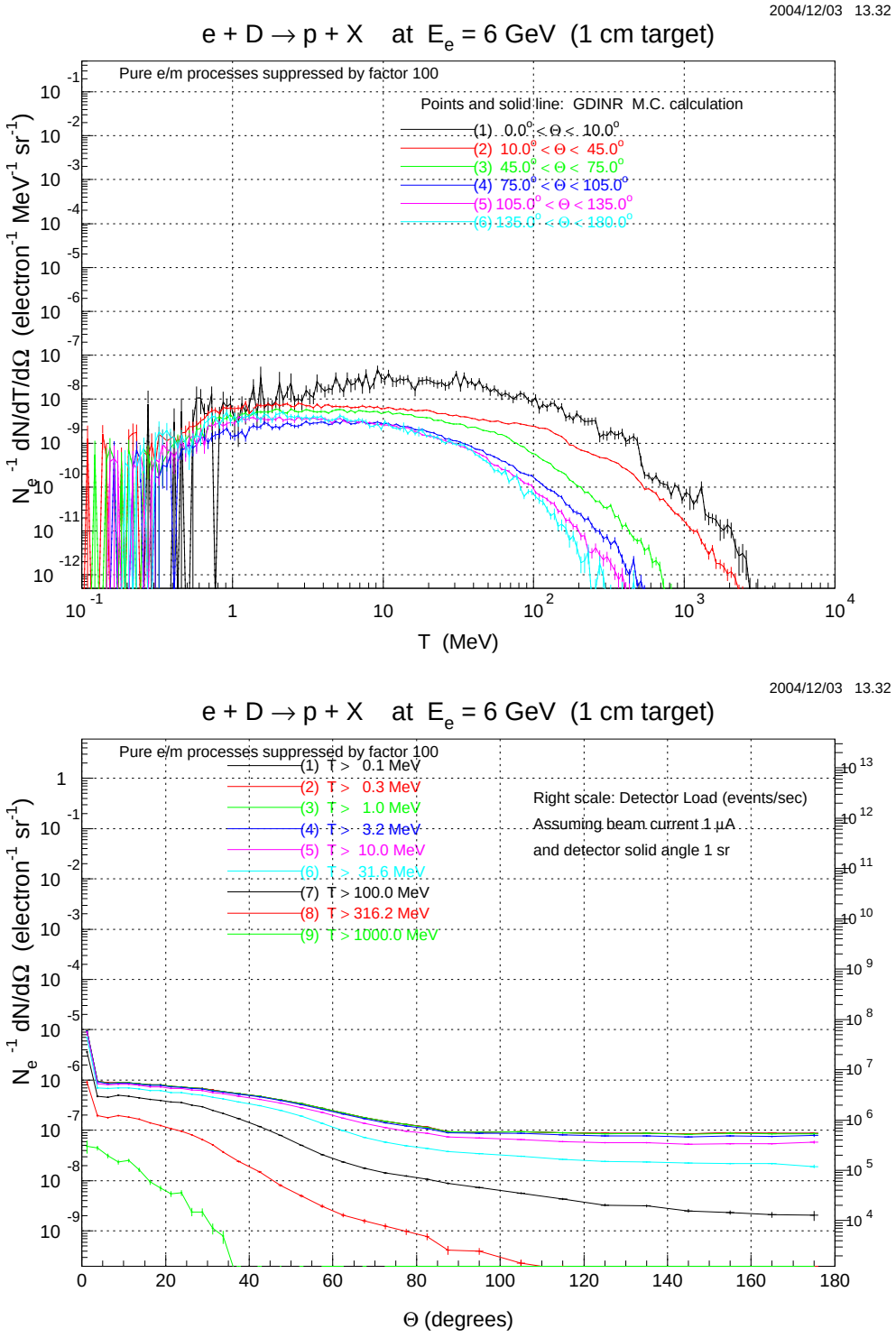

Figure 7: Monte-Carlo results for proton background for the proposed experiment per sr.

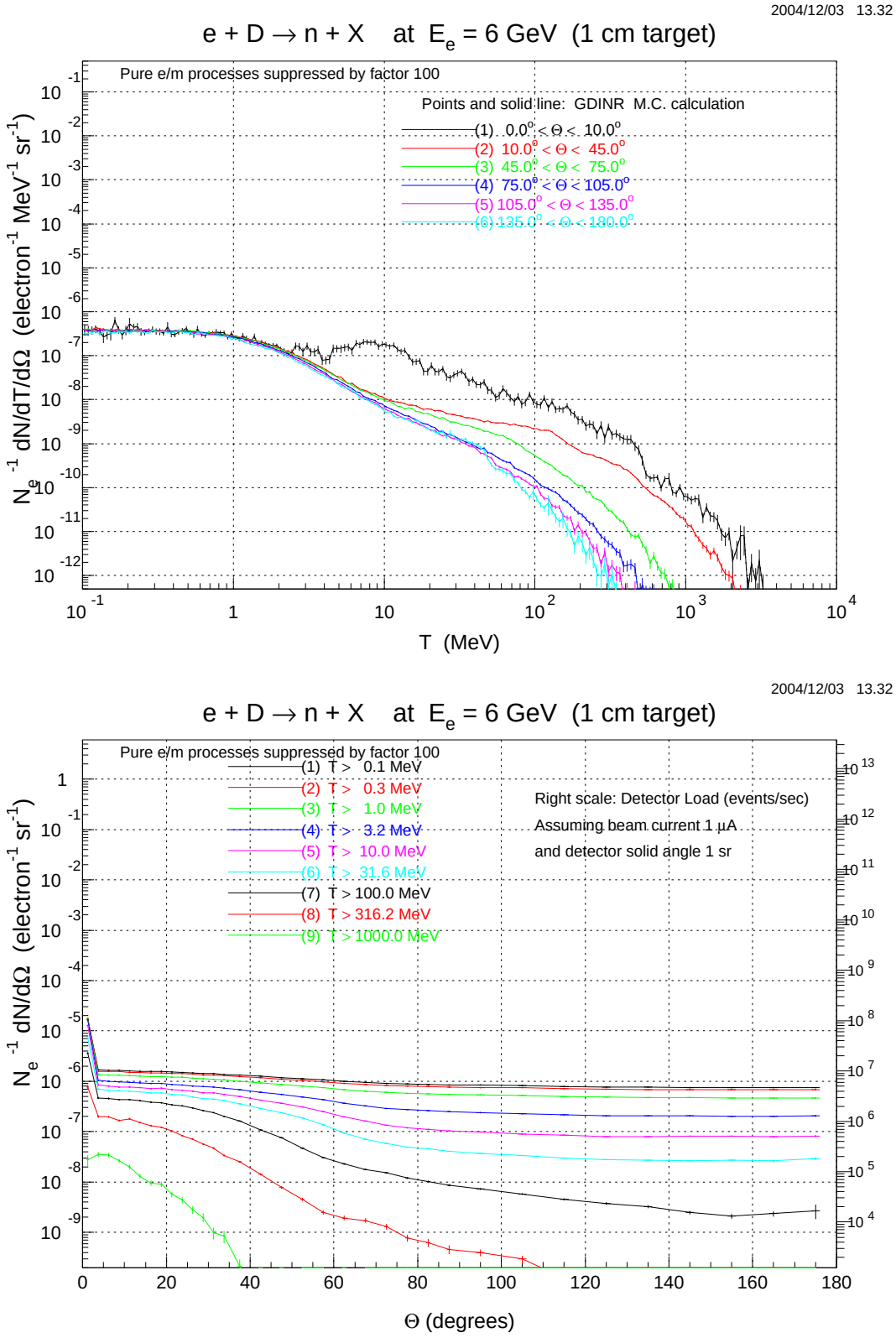

Figure 8: Monte-Carlo results for neutron background for the proposed experiment per sr.

Figure 8 shows the Monte-carlo simulation of expected background neutron rates. Interactions of the target with primary electrons as well as with real and quasi-real photons accompanying the beam have been considered in this Monte-Carlo. The signal to noise ratio analysis for different neutron momentum ranges is presented in table 1. The second column of the table shows simulated background rates (evaluated for the proposed luminosity and neutron detector solid angle), for several ranges of neutron kinetic energies considered in this proposal.

Let the background neutron rate for a momentum range Δp be $B_{\Delta p}$. Then the probability of getting a background neutron in momentum range Δp followed by a beam bunch that produced a detected electron is given by $B_{\Delta p}/(20 \times 10^6)$ (for the proposed 20 MHz beam structure). This per pulse background hit probability is given in the third column of the table. The probability of getting a real coincidence for a neutron in the momentum range Δp is given by

$$Pr_{real} = S_{\Delta p} \frac{\Delta\Omega}{4\pi} \frac{F_{2,p}}{(F_{2,p} + F_{2,n})}, \tag{16}$$

where $S_{\Delta p}$ is the integrated strength of the (normalized) neutron momentum distribution over Δp, $\Delta\Omega$ is the neutron detector solid angle and $F_{2,p}$ and $F_{2,n}$ are the proton and the neutron structure functions. [2] This signal probability is given in the forth column of the table followed by the signal to noise ratio in the fifth column.

Kinetic energy range MeV	Background n rate s^{-1}	Background probability	Signal probability	signal to noise ratio
1 - 3.2	3.4×10^6	1.7×10^{-1}	1.1×10^{-1}	1:1.6
3.2 - 10	2.6×10^6	1.3×10^{-1}	8.7×10^{-2}	1:1.5
10- 20	9×10^5	4.5×10^{-2}	2.9×10^{-2}	1:1.6
20- 50	5×10^5	2.4×10^{-2}	1.7×10^{-2}	1:1.5
50- 79	1×10^5	4.5×10^{-3}	3.3×10^{-3}	1:1.4

Table 1: Signal to noise ratio analysis for different neutron momentum ranges.

As the table indicates, the signal to noise ratio over the entire momentum range of the neutron is about 1:1.5. We will use the multi-hit feature of the TDCs to measure the background with high accuracy. A multi-hit TDC with a gate width of about 1 μs will register random coincidence spectra for 20 beam bunches following a bunch that generates an electron hit. This will allow us to determine the background level at every neutron momentum with a statistical error about 4 times smaller than the statistical error we project for the signal. Thus at the projected signal to noise ratio of 1:1.5, our statistical error will increase only by a factor of $\sqrt{2.5}$ due to background subtraction. This uncertainty was factored into all projected statistical errors given in this proposal.

For the detection of neutrons with kinetic energies between 15 MeV and 65 MeV we will use the GEn neutron detector installed behind the neutron-hemisphere. This

[2] Note that the neutron detection efficiency enters both probabilities and drops out of the signal to noise ratio.

detector will be at an average distance of 2.5 meters from the target and will cover a solid angle of about 4 sr.

3.6.1 Low energy neutron detector hardware

We are considering two options for low energy neutron detector hardware; a system based on 5 cm thick slabs of plastic scintillator or a system based on liquid scintillator. We will evaluate both options carefully during a facility development run we are planing for April 2005.

A neutron detector very similar to the one proposed for this experiment was recently constructed[53] by Blaine Norum and Brad Sawatzky, members of this collaboration from the University of Virginia group. This low energy neutron detector, nicknamed **BLOWFISH** was successfully used to detect neutrons with kinetic energies as low as 0.65 MeV in a low energy D(γ,n) experiment at **HIGS**. The BLOWFISH detector (Fig 9) consists of 88 BC-505 liquid scintillator cells mounted on the surface of a 40 cm radius imaginary sphere. Each cell (Fig 10) consists of a scintillation box $8.2 \times 8.2 \times 7.1$ cm^2 constructed of Lucite. The scintillation box is coupled through a light guide to the PMT and the base.

Liquid scintillators are known for their obnoxious chemical properties and hazardously low flash points. However, liquid scintillator BC-505 was found to be much easier to work with than the more traditional liquid scintillator NE-213. Furthermore BC-505 has a higher flash point than NE-213 and allows safer working conditions.

The BLOWFISH detector was successfully commissioned and operated in 2002. The experimentally measured neutron detection efficiencies for BLOWFISH cells agree well with the simulations and are around 40% for neutrons with kinetic energies above 1 MeV.

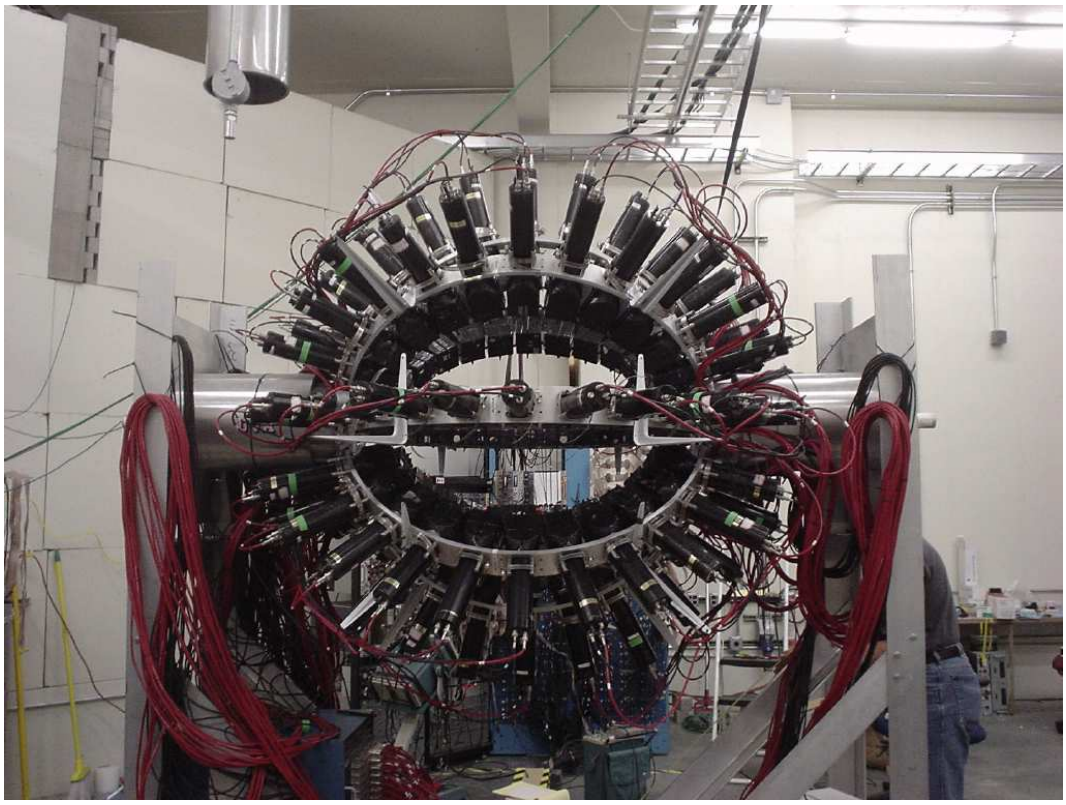

Figure 9: BLOWFISH low energy neutron detector at HIGS.

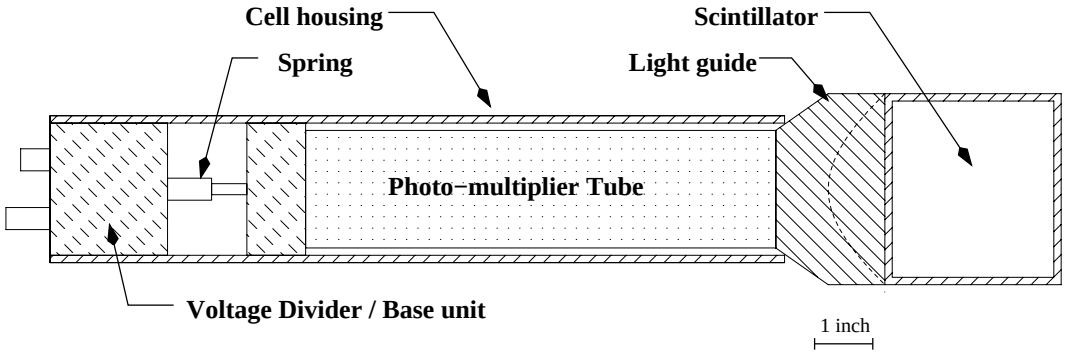

Figure 10: A single neutron cell from BLOWFISH.

The expertise of Blaine Norum and Brad Sawatzky in the design, construction and successful operation of the ultra-low energy neutron detectors would be invaluable in the construction of neutron detectors for the proposed experiment. Here we present a cost analysis for the proposed neutron detector assuming that we will choose liquid scintillators. The cost for a plastic scintillator based system will be comparable. The active area of the proposed neutron hemisphere is approximately 1 m^2, and it will consist of roughly 175 BLOWFISH-type cells. Table 2 shows the estimated

cost of 175 assembled cells, based on the very recent experience of the University of Virginia group. Allowing a 35% increase to meet inflation and contingency and adding $ 30,000 to cover the cost of 175 TDC and ADC channels, the total cost of the proposed neutron detector is expected to be less than $ 150,000.

Quantity	Description	Unit Cost	Sub total
15 gal	BC-505 liquid scintillator	$300	$4,500
175	PMT	$250	$43,750
175	Base+housing units	$175	$30,625
175	Lucite box + light guide	$50	$8,750
175	fiber optics for gain monitor	$15	$2,625
			$90,250

Table 2: Breakdown of estimated costs for the proposed neutron detector.

3.6.2 Low energy neutron detector tests

The **HIGS** facility shutdown scheduled for 2005 allows us to borrow several BLOWFISH neutron detector cells to test in beam in Hall A. We have already made a request to Hall A leader for 24 hours of beam time during facility development time in April 2005. This is during the short-range correlation experiment in Hall A when the BigBite spectrometer will be operational.

We plan to conduct this test with the 32 ns G0 beam structure to test the neutron detection technique. We will use the 4 cm deuteron target with several beam currents ranging from 0.2 μA to 10 μA. We will test four BLOWFISH neutron cells, four plastic scintillator based cells and four Gen neutron bars in this run. We will compare liquid cells with plastic cells based on parameters such as the light output and response time and will decide which type to use for the proposed experiment.

Furthermore, with the PAC endorsement of this proposal, this collaboration will seek funding for a prototype neutron detector that covers 1/4 solid angle of the full proposed detector in the next few months. We are planing to design, construct and test this prototype detector in the Summer of 2005.

3.7 Neutron momentum resolution

The neutron momentum resolution for the proposed system will be limited by the thickness of the scintillator compared to the distance to the target. With a 5 cm scintillator slab located at 50 cm from the target, the standard deviation for the momentum measurement for these non-relativistic neutrons will be

$$\sigma(p) = 1/\sqrt{12} \times \text{thickness/distance} \approx 2.9\% \qquad (17)$$

The time resolution of the TOF measurement will be around 250 ps and will not dominate the momentum resolution even for the fastest neutrons (TOF= 9.5 ns).

3.8 Systematic Errors

As we have described in the previous sections, most of the systematic errors that affect absolute cross section measurements cancel out when we form the cross section ratio G as defined in Equation 14. Our cross sections are normalized inclusive $D(e,e')$ cross sections. The deuteron structure functions have been measured to 1% level in the proposed kinematic range. Since we are only sensitive to the relative uncertainty in the deuteron structure functions, the uncertainty contribution contribution towards G would be even smaller than 1%. However we will use 1% as a safe upper limit for the uncertainty in the raw cross section ratio G_{raw}.

The extra statistical error due to random background subtraction has already been factored in to the statistical error of G_{raw} given in tables 5 and 6. However, the radiative corrections and subtraction of physics background we have to do to go from the raw cross section ratio G_{raw} to the corrected cross section ratio G will contribute to the final systematic uncertainty.

In the spectator picture, the radiation from the electron before and after scattering off the bound proton is independent of the spectator neutron. Therefore we can use the inclusive radiative correction procedures perfected at SLAC. Here we will perform the correction for each α^{sp} bin separately using the correct invariant variable x' calculated taking the momentum of the proton into account. As was realized in SLAC and Jefferson Lab inclusive experiments [2, 3, 57] the inclusive radiative correction can be applied to an accuracy of about 1% of the final cross-section. Thus we estimate the uncertainty due to radiative correction in the final cross section ratio to be 1% or better.

As we discuss earlier, we expect the main physics background to be the Sullivan process, at less than 2% level of the signal. With the H$(e,e'n)$ data we are proposing to take we will be able to correct correct this background to better than 0.5%.

Table 3 summarizes the systematic errors we expect in the final cross section ratio G. We would like to emphasize that the relative uncertainty between different x', α^{sp} points we measure will be smaller than the overall uncertainty given here.

Source	$\delta G/G$
Normalization to inclusive $D(e,e')$	1%
Radiative corrections	1%
Physics background subtraction	0.5%
Total estimated systematic uncertainty, added in quadrature	1.5%

Table 3: Estimated systematic error in the final cross section ratio G.

3.9 Kinematics and rate estimates

All kinematic settings for this experiment are with $E_0 = 6$ GeV and $\theta_e = 35°$. We have assumed a luminosity of 5×10^{35} cm^{-2}s^{-1} achieved with a 1 cm thick liquid deuterium target and an average beam current of 0.8 μA. We have used a solid angle of 96 msr for the BigBite spectrometer at 35°. A kinematic cut at $p_t < 0.2$ GeV/c was used to ensure that the transverse momentum was small. To select DIS events, $Q^2 > 1$ GeV^2 and $W'^2 > 4$ GeV^2 cuts will be used. An average neutron efficiency of 30% was assumed.

Table 4 shows the beam time allocation for different settings. Tables 5 and 6 give the Q^2, W'^2 and statistics for each x', α^{sp} bin for the low and higher neutron momentum settings respectively.

setting	Description	Target	Neutron momentum	Neutron Detector	Time (Hours)
I	low n momentum $D(e,e'n)$	LD2	0.05-0.17 GeV/c	Neutron hemisphere	75
II	higher n momentum $D(e,e'n)$	LD2	0.15-0.4 GeV/c	Gen detector	300
I.a	low n momentum $H(e,e'n)$	LH2	0.05-0.17 GeV/c	Neutron hemisphere	5
II.a	higher n momentum $H(e,e'n)$	LH2	0.15-0.4 GeV/c	Gen detector	30
	System checkout				20
	Total				430

Table 4: Beam time breakdown for production and background running as well as experimental setup checks

α^{sp}	E′ (GeV)	Q^2 (GeV/c)^2	x'	W'^2 (GeV/c^2)^2	Rate (events per hour)	Total counts	Stat. uncertainty
1.04	0.45	0.98	0.10	10.0	3200	240000	0.003
1.04	0.60	1.30	0.13	9.4	2700	190000	0.004
1.04	0.75	1.63	0.17	8.8	2300	170000	0.004
1.04	0.90	1.95	0.21	8.2	2000	150000	0.004
1.04	1.05	2.28	0.25	7.6	1750	130000	0.004
1.04	1.20	2.60	0.30	7.0	1530	110000	0.005
1.04	1.35	2.93	0.35	6.4	1300	100000	0.005
1.04	1.50	3.26	0.40	5.8	1090	80000	0.006
1.04	1.65	3.58	0.45	5.2	880	65000	0.006
1.04	1.80	3.91	0.51	4.6	670	51000	0.007
1.04	1.95	4.23	0.58	4.0	500	40000	0.008
1.04	2.10	4.56	0.65	3.4	330	26000	0.010
1.10	0.50	1.09	0.11	9.3	850	64000	0.006
1.10	0.65	1.41	0.15	8.7	720	53000	0.007
1.10	0.80	1.74	0.19	8.1	620	46000	0.007
1.10	0.95	2.06	0.24	7.5	540	40000	0.008
1.10	1.10	2.39	0.28	6.9	470	35000	0.009
1.10	1.25	2.71	0.33	6.3	400	30000	0.009
1.10	1.40	3.04	0.39	5.7	330	25000	0.010
1.10	1.55	3.36	0.44	5.1	270	20000	0.011
1.10	1.70	3.69	0.50	4.5	210	15000	0.013
1.10	1.85	4.01	0.57	4.0	150	11500	0.015
1.10	2.00	4.34	0.64	3.4	110	8000	0.018
1.15	0.55	1.19	0.13	8.6	1000	76000	0.006
1.15	0.70	1.52	0.18	8.0	860	64000	0.006
1.15	0.85	1.84	0.22	7.5	740	55000	0.007
1.15	1.00	2.17	0.27	6.9	640	48000	0.007
1.15	1.15	2.50	0.32	6.3	550	41000	0.008
1.15	1.30	2.82	0.37	5.7	460	34000	0.009
1.15	1.45	3.15	0.42	5.1	370	28000	0.010
1.15	1.60	3.47	0.49	4.6	290	22000	0.011
1.15	1.75	3.80	0.55	4.0	210	16000	0.013
1.15	1.90	4.12	0.62	3.4	150	11000	0.015

Table 5: Expected results from setting I (75 hours) for each x', α^{sp} bin. The statistics given have been calculated using the neutron detector solid angle (4 sr), neutron detection efficiency (30%), and the deuteron spectral strength integrated over the α^{sp} bin width. A $p_t < 0.2$ GeV/c has been applied. The statistical errors shown include an extra factor of $\sqrt{2.5}$ to account for the random background subtraction uncertainty.

α^{sp}	E′ (GeV)	Q^2 (GeV/c)^2	x'	W'^2 (GeV/c^2)^2	Rate (events per hour)	Total counts	Stat. uncertainty
1.22	0.45	0.98	0.11	8.5	100	25000	0.009
1.22	0.60	1.30	0.16	7.9	80	24000	0.010
1.22	0.75	1.63	0.20	7.3	70	21000	0.011
1.22	0.90	1.95	0.25	6.8	60	18000	0.012
1.22	1.05	2.28	0.30	6.2	50	15000	0.013
1.22	1.20	2.60	0.35	5.6	42	13000	0.014
1.22	1.35	2.93	0.41	5.1	34	10000	0.016
1.22	1.50	3.26	0.47	4.5	27	8000	0.018
1.22	1.65	3.58	0.54	4.0	20	6000	0.021
1.22	1.80	3.91	0.61	3.4	14	4200	0.025
1.30	0.47	1.02	0.13	7.9	31	9000	0.017
1.30	0.62	1.35	0.17	7.3	26	7700	0.018
1.30	0.77	1.67	0.22	6.8	22	6600	0.020
1.30	0.92	2.00	0.27	6.2	19	5600	0.021
1.30	1.07	2.32	0.33	5.6	16	4700	0.023
1.30	1.22	2.65	0.39	5.1	13	3800	0.026
1.30	1.37	2.97	0.45	4.5	10	3000	0.029
1.30	1.52	3.30	0.52	4.0	8	2300	0.034
1.30	1.67	3.62	0.59	3.4	5	1600	0.040
1.40	0.40	0.87	0.11	7.6	18	5500	0.022
1.40	0.60	1.30	0.18	6.9	14	4200	0.025
1.40	0.80	1.74	0.25	6.2	11	3300	0.028
1.40	1.00	2.17	0.32	5.4	9	2600	0.031
1.40	1.20	2.60	0.40	4.7	7	2000	0.036
1.40	1.40	3.04	0.49	4.0	5	1400	0.043
1.40	1.60	3.47	0.59	3.3	3	860	0.054

Table 6: Same as in table 4, for setting II (300 hours).

Figure 11 shows the projected uncertainties for the semi-inclusive cross section ratio G (defined in equation 15) for each α^{sp} bin as a function of x'.

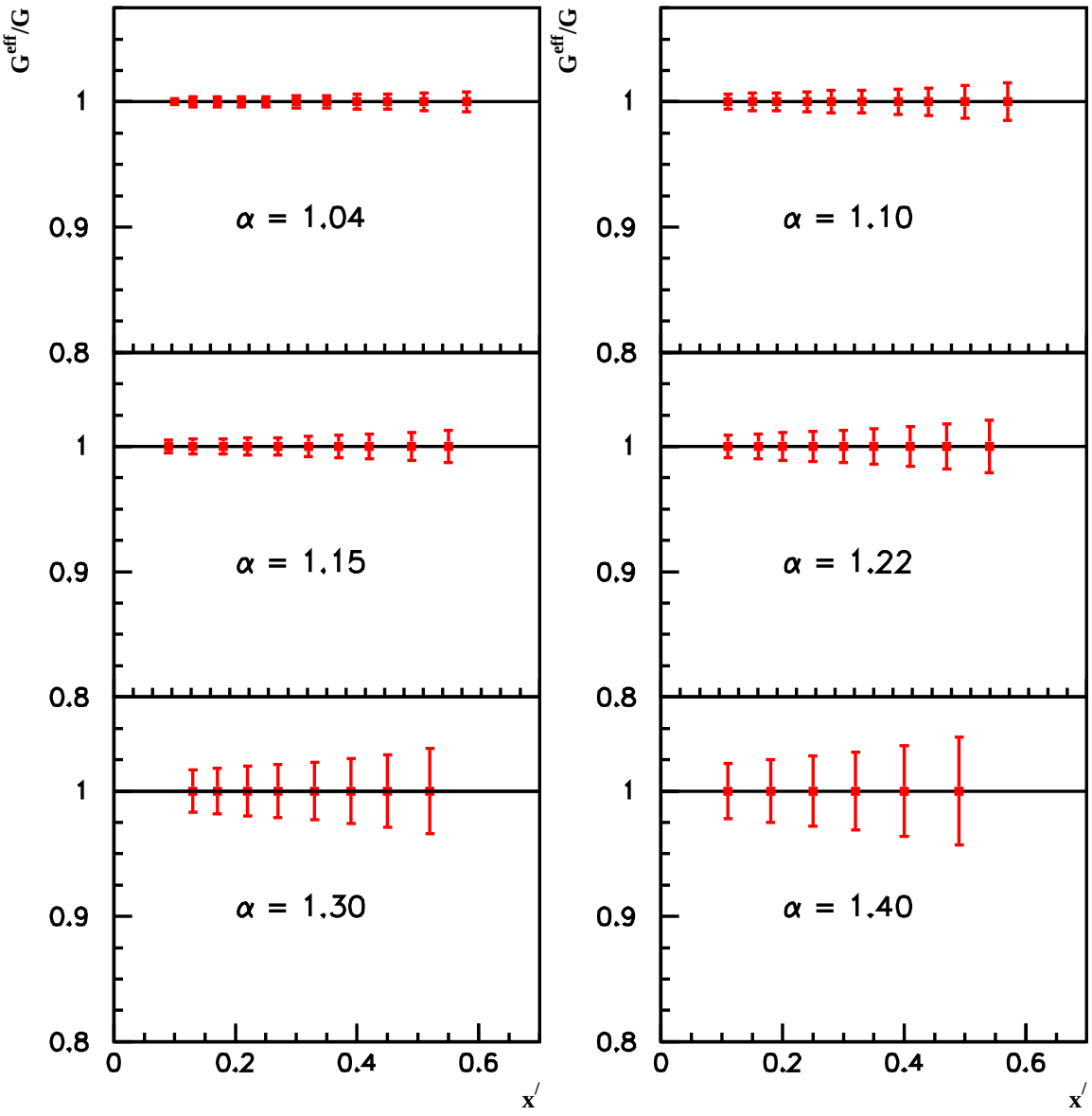

Figure 11: Projected uncertainties for the semi-inclusive cross section ratio G for each α^{sp} as a function of x'. All points shown here are after applying DIS cuts: $Q^2 > 1$ GeV^2 and $W'^2 > 4$ GeV^2.

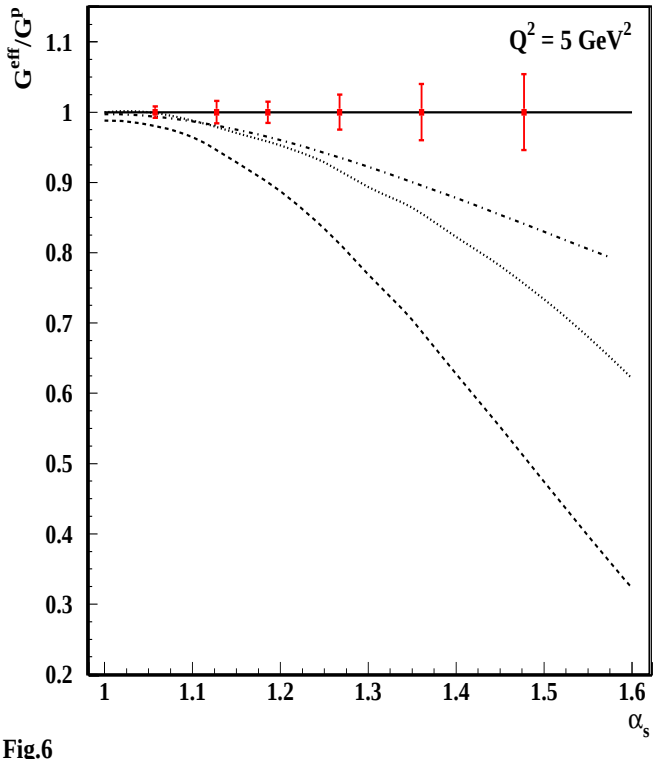

Figure 12: Projected uncertainties for the $x' = 0.6$ points. Theory curves from Melnitchouk *et al.*, evaluated at $Q^2 = 5$ GeV/c^2 : Dashed: PLC suppression model; Dotted: Rescaling model, Dot-dashed: nuclear binding model. Note that the W'^2 cut was slightly relaxed to $W'^2 > 3.4$ (or $W' > 1.84$) to obtain these points.

As presented in Table 4, we request 430 hours (just 18 days) for the proposed measurement. In addition to this, we would like to request 48 hours of facility development time before the experiment to commission the neutron detector.

The projected statistical errors for most of the high x' and high α^{sp} points are significantly greater than the estimated systematic error given in Table 3. Thus we have much room to improve the overall accuracy of these very interesting kinematic points. For example, for a 40 day measurement the uncertainty of the three higher α^{sp} points shown in Fig. 12 will be smaller by a factor of 1.7. However, since this experiment is the first of its kind, and there is a real possibility now of getting 12 GeV beam in the next several years, we will only request 430 hours needed for respectable statistics at this time. Based on the success of this measurement we will be able to prepare a very strong experimental program for 12 GeV to probe the EMC effect up to $x' \sim 0.8$ in the DIS region.

4 Summary and Request

We are proposing a measurement of the ratio between the D$(e, e'$n$)$X cross section at a given x and the D$(e, e'$n$)$X cross section at $x = 0.2$. This ratio will be measured over

a grid of the scaling variable x and the recoil neutron momentum in the DIS region up to $x < 0.6$. This allows us to study the variation of the effective structure function $F_{2,p}^{eff}$ for the bound proton as a function of the spectator neutron momentum. This precision measurement of the evolution of $F_{2,p}^{eff}$ will allow a clear distinction between different theoretical explanations on the origin of the EMC effect. This may provide crucial clues to solve a mystery that has puzzled both the nuclear and particle physics communities for over twenty years. Given the success of the proposed experiment, it has the potential to open up an important experimental initiative at 12 GeV to probe the EMC effect up to $x \sim 0.8$.

We are requesting 430 hours to perform this breakthrough measurement.

References

[1] J. J. Aubert *et al.* (EM Collaboration), Phys. Lett. B **123**, 275 (1983).

[2] S. Dasu *et al.*, Phys. Rev. D **49**, 5641 (1994).

[3] J. Gomez *et al.*, Phys. Rev. D **49**, 4348 (1994).

[4] A. C. Benvenuti *et al.* (BCDMS Collaboration), Phys. Lett. B **189**, 483 (1987).

[5] J. Ashman *et al.* (EM Collaboration), Phys. Lett. B **202**, 603 (1988); Z. Phys. C **57**, 211 (1993).

[6] D. F. Geesaman, K. Saito and A. W. Thomas, Ann. Rev. Nucl. Part. Sci. **45**, 337 (1995).

[7] J. Arrington (Spokesperson), Jefferson Lab Experiment 03-103.

[8] W. Melnitchouk, M. Sargsian and M. I. Strikman, Z. Phys. A **359**, 99 (1997)

[9] S. E. Kuhn and K. A. Griffioen (Spokespersons), Jefferson Lab Experiment 94-102.

[10] W. Melnitchouk and A. W. Thomas, Phys. Lett. B **377**, 11 (1996).

[11] W. Melnitchouk and A.W. Thomas, Z. Phys. **A 353** (1995) 311; W. Melnitchouk private communications.

[12] H. Fenker, C. Keppel, S. E. Kuhn and W. Melnitchouk (Spokespersons), Jefferson Lab Experiment 03-012

[13] Proceedings of Workshop "Future Physics at HERA", Sep. 95 – May 96, DESY, Hamburg (1996); G. van der Steenhoven, private communication.

[14] L. L Frankfurt and M. I. Strikman, Phys. Rep. **76**, 217 (1981).

[15] W. Melnitchouk, A. W. Schreiber, and A. W. Thomas, Phys. Rev. D **49**, 1183 (1994).

[16] S. A. Kulagin, G. Piller, and W. Weise, Phys. Rev. C **50**, 1154 (1994).

[17] W. Melnitchouk, A. W. Schreiber, and A. W. Thomas, Phys. Lett. B **335**, 11 (1994).

[18] S. A. Kulagin, W. Melnitchouk, G. Piller, and W. Weise, Phys. Rev. C **52**, 932 (1995).

[19] W. W. Buck and F. Gross, Phys. Rev. D **20**, 2361 (1979); J. W. Van Orden, N. Devine, and F. Gross, Phys. Rev. Lett. **75**, 4369 (1995); E. Hummel and J. A. Tjon Phys. Rev. C **49**, 21 (1994).

[20] W. Melnitchouk, G. Piller, and A. W. Thomas, Phys. Lett. B **346**, 165 (1995); G. Piller, W. Melnitchouk, and A. W. Thomas, Phys. Rev. C **54**, 894 (1996).

[21] L. L. Frankfurt and M. I. Strikman, Phys. Lett. **64** B, 435 (1976).

[22] P. V. Landshoff and J. C.Polkinghorne, Phys. Rev. D **18**, 158 (1978).

[23] L. L. Frankfurt and M. I. Strikman, Phys. Rep. **160**, 235 (1988).

[24] G. P. Lepage and S. J. Brodsky, Phys. Rev. D **22**, 2157 (1980).

[25] M. Lacombe *et al.*, Phys. Rev. C **21**, 861 (1990).

[26] R. Machleidt, K. Holinde, and Ch. Elster, Phys. Rep. **149**, 1 (1987).

[27] M. I. Strikman, M. Tverskoy, and M. Zhalov, in Proceedings of Workshop "Future Physics at HERA", Hamburg, pp.1085-1088 (1996), nucl-th/9609055.

[28] E665 Collaboration, M. R. Adams *et al.*, Phys. Rev. Lett. **74**, 5198 (1995).

[29] L. L. Frankfurt, G. A. Miller, W. R. Greenberg, M. M. Sargsyan, and M. I. Strikman, Z. Phys. A **352**, 97 (1995).

[30] L. L. Frankfurt, G. A. Miller, W. R. Greenberg, M. M. Sargsyan, and M. I. Strikman, Phys. Lett. B **369**, 201 (1996).

[31] L. L. Frankfurt and M. I. Strikman, Nucl. Phys. **B250**, 1585 (1985).

[32] C. Ciofi degli Atti, L. P. Kaptari and B. Z. Kopeliovich, Eur. Phys. J. A **19**, 145 (2004) [arXiv:nucl-th/0307052].

[33] C. E. Carlson and K.E. Lassilla and P.U. Sukhatme, Phys. Lett. B **263**, 277 (1992).

[34] C. Ciofi degli Atti and S. Simula, Few Body Systems **18**, 55 (1995).

[35] S. V. Akulinichev, S. A. Kulagin and G. M. Vagradov, Phys. Lett. **158** B, 485 (1985); S. A. Kulagin, Nucl. Phys. **A500**, 653 (1989).

[36] G. V. Dunne and A. W. Thomas, Nucl. Phys. **A446**, 437c (1985).

[37] M. Ericson and A. W. Thomas, Phys. Lett. B **128**, 112 (1983).

[38] B. L. Friman, V. R. Pandharipande, and R. B. Wiringa, Phys. Rev. Lett. **51**, 763 (1983); E. L. Berger, F. Coester, and R. B. Wiringa, Phys. Rev. D **29**, 398 (1984).

[39] H. Jung and G. A. Miller, Phys. Lett. B **200**, 351 (1988).

[40] C. Ciofi degli Atti and S. Liuti, Phys. Lett. B **225**, 215 (1989).

[41] L. P. Kaptari *et al.*, Nucl. Phys. **A512**, 684 (1990); W. Melnitchouk and A. W. Thomas, Phys. Rev. D **47**, 3783 (1993).

[42] R. P. Bickerstaff and A. W. Thomas, J. Phys. G **15**, 1523 (1989).

[43] S. Huang and J. Tjon, Phys. Rev. C **49**, 1702 (1994); N. Ishii, W. Bentz, and K. Yazaki, Phys. Lett. B **301**, 165 (1993); H. Meyer, Phys. Lett. B **337**, 37 (1994); C. M. Shakin and W.-D. Sun, Phys. Rev. C **50**, 2553 (1994).

[44] M. R. Frank, B. K. Jennings and G. A. Miller, Phys. Rev. C **54**, 920 (1996).

[45] L. L. Frankfurt M. M. Sargsian and M. I. Strikman, Z. Phys. A **335**, 431 (1990).

[46] F. E. Close, R. G. Roberts and G. G. Ross, Phys. Lett. B **129**, 346 (1983).

[47] O. Nachtmann and H. J. Pirner, Z. Phys. C **21**, 277 (1984).

[48] R. L. Jaffe, F. E. Close, R. G. Roberts and G. G. Ross, Phys. Lett. B **134**, 449 (1984).

[49] F. E. Close *et al.*, Phys. Rev. D **31**, 1004 (1985).

[50] G. Güttner and H. J. Pirner, Nucl. Phys. **A457**, 555 (1986).

[51] G. Cates, K. McCormick, B. Reitz, and B. Wojtsekhowski, Jefferson Lab experiment E02-013.

[52] C. Ciofi degli Atti and S. Simula, Phys. Lett. B **319** (1993) 23.

[53] B. Swatski, Ph. D Thesis, University of Virginia (2004).

[54] P. Degtiarenko, Private Communications.

[55] P. Degtiarenko, Private Communications.

[56] S. Simula, Phys. Lett. B **387**, 245 (1996)

[57] L. W. Whitlow, Ph. D Thesis, Stanford University (1990) (SLAC-0357); L. W. Whitlow, E. M. Riordan, S. Dasu, S. Rock and A. Bodek, Phys. Lett. B **282**, 475 (1992).

[58] G. Levman, Nucl. Phys. B **642**, 3 (2002). [arXiv:hep-ph/0208059].; K. Borras [H1 and ZEUS Collaborations], Acta Phys. Polon. B **33** (2002) 3219.

[59] H. Jung, Comput. Phys. Commun. **86**, 147 (1995).